ISSN 1582-9596

# Environmental Engineering and Management Journal



"Gheorghe Asachi" Technical University of Iasi

## Editorial Board



## Scientific Advisory Board

**Environmental Engineering and Management Journal**
**August 2020, Vol. 19, No. 8, 1261-1458**

**Contents**

*Environmental Engineering and Management Journal*

*August 2020, Vol. 19, No. 8, 1299-1308*
*http://www.eemj.icpm.tuiasi.ro/; http://www.eemj.eu*

*"Gheorghe Asachi" Technical University of Iasi, Romania*

# ISOTHERMAL AND KINETIC ADSORPTION OF ANIONIC DYE ONTO IMPREGNATED SILICA GELS WITH ALUMINUM

**Yudi Aris Sulistiyo[1*], Faizatur Rofi'ah[1], Suwardiyanto[1], Ari Satia Nugraha[2], Zulfikar[3], Gagus Ketut Sunnardianto[4]**

*[1]Inorganic Material for Energy and Environment Research Group, Department of Chemistry, Faculty of Mathematics and Natural Science, University of Jember, Jember, Indonesia 68121*
*[2]Drug Utilisation and Discovery Reseach Group, Faculty of Pharmacy, University of Jember, Jember, Indonesia 68121*
*[3]Sensor and Chemical Instrumentation Research Group, Department of Chemistry, Faculty of Mathematics and Natural Science, University of Jember, Jember, Indonesia 68121*
*[4]Research Center for Chemistry, Indonesian Institute of Sciences (LIPI), Kawasan Puspitek Serpong, Tangerang Selatan, 15314, Indonesia*

**Abstract**

Impregnation of aluminium ion onto silica gel (SG) surface (Al/SG) is to increase the adsorption capacity of an anionic dye such as Indigo carmine (IC). The impregnation was carried out using wetness impregnation. The change of the functional group was evaluated by FTIR, crystallinity was determined using XRD, surface morphology were studied by SEM-EDX, while surface area and pore size using $N_2$ gas adsorption-desorption analyzer. Meanwhile, the best of IC adsorption condition onto SG and Al/SG occurred consecutively at pH 2 and 3. The optimum adsorption of both adsorbent was 25.707 and 88.143 $mg.g^{-1}$ with the adsorption efficiency 21.82% and 80.47%, respectively. Whereas, isothermal adsorption model of SG and Al/SG consecutively followed Langmuir and Freundlich model. The equilibrium adsorption was achieved in 60 min of contact time following pseudo-second order kinetic model. This study provides information about the replacing negative charge in the surface of the adsorbent with cation would increase the adsorption capacity of the anionic adsorbate.

*Key words:* adsorption isotherm, adsorption kinetic, aluminum impregnation, anionic dye indigo carmine, modified silica gels

*Received: August, 2019; Revised final: March, 2020; Accepted: April, 2020; Published in final edited form: August, 2020*

## 1. Introduction

Industrial coloring activities such as textiles, printing, paper, and plastic used approximately 50% of the anionic dyes (Alver and Metin, 2012; Zhou et al., 2019). In the coloring process, they would discharge about 10-15% unused dye into the aquatic environment as wastes (Mahmoodi et al., 2011a). Even at low concentrations, the anionic dye is colorful and challenging to be degraded naturally (Chen and Chen, 2018; Ma et al., 2011). The anionic dye is one of the acidic dyes that highly reactive, harmful to the environment, and carcinogenic to humans (Jiang et al., 2019; Tang et al., 2019). Indigo Carmine is also a group of anionic indigoid dyes with high toxicity levels and skin and eye irritant (Carvalho et al., 2011).

Biological, chemical and physical methods are used to solve anionic dye problems. The biological methods such as bioremediation and biodegradation by microorganisms are the most eco-friendly (Mishra and Malik, 2014; Wangpradit and Chitprasert, 2014), but the degradation rates of the dye were generally slow (Amir et al., 2017). The advantage using chemical methods i.e. coagulation, flocculation, oxidation, ozonation, electrochemical, and photo-degradation are usually efeective, but they have the

* Author to whom all correspondence should be addressed: e-mail: yudi.fmipa@unej.ac.id; Phone: +62331334293; Fax: +62331330225

problems such as produce sludge, need large amounts of chemical reagent, need high energy and technically difficult to apply (Zhou et al., 2019). Meanwhile, the physical treatment such as filtration with the membrane and adsorption was good removal of wide variety of dye and relatively easy to implement (Salleh et al., 2011). Adsorption is the most promising method to solve the anionic dye problems because its technology is easy, inexpensive, effective, and does not generate new environmental problems (Silva et al., 2013). On its process, adsorption needs materials that have high sorption capacity for anionic dye.

The most economical adsorbent is natural materials such as zeolite, fly ash, clay, active carbon, and biomass. The optimum removal of ramazol red dye was 11.83 $mg.g^{-1}$ that determined by the $SiO_2$ content of the adsorbent (Costa and Paranhos, 2019). On the other hand, Fly ash that has $SiO_2$ content around 64.97% was a potential adsorbent to remove dye pollutants (Adak et al., 2014). Fly ash was produced from coal combustion of power plant around 750 million tons in 2015 (Yao et al., 2015), and only 12% was recycled into useful products (Gollakota et al., 2019). So, the utilization of fly ash as adsorbent is not only able to solve the dye pollutants problem, but also the coal combustion waste problem. However, the metal oxides contained in the fly ash can decrease the sorption capacity of dye. It was shown in the adsorption capacity of methylene blue by fly ash, and amorphous silica from fly ash was 0.12 $mg.g^{-1}$ (Karaca et al., 2018) and 323.63 $mg.g^{-1}$ (Yuan et al., 2019), respectively. Hence conversion fly ash to be silica gels is a potential method to produce a material having excellent performance as the adsorbent (Manchanda et al., 2017). Moreover, silica has high thermal and chemical stability, possible reuse, relatively rapid to obtain the equilibrium, and high surface area (Mahmoodi et al., 2011b).

The primary challenge to apply the adsorbent to the anionic dyes is the negative charge from the surface of the material. The negative charge of the surface of silica was from Si-O and Si-OH group, which suitable for the positive charge of adsorbate and prevented negative charge (Anbia et al., 2010). The negative charge of the material causes a repulsive force with the anionic dye. It is certainly not beneficial and requires a transformation of the surface charge of the material from negative to positive. The modification of the surface charge can be carried out using metal impregnation.

Aluminum with amphoteric nature can be chosen as an excellent modifier because it has a wide range of pH tolerance. The previous study showed that the addition of Aluminum 10% onto SBA-15 be able to adsorb anionic phosphate about 862 $mol.g^{-1}$, while without impregnation SBA-15 cannot adsorb the phosphate due to the negative charge of SBA-15 (Shin et al., 2004). In this paper, a study of the indigo carmine uptake as the representation of anionic dye was carried out using impregnated aluminum ion onto silica gel. The silica gel was prepared from fly ash from a power plant combustion. The adsorption is evaluated by toward pH, initial concentration of indigo carmine, and contact time of adsorption in batch systems. The performance of the adsorbents was studied by the isothermals and kinetic models of adsorption.

## 2. Experiments

### *2.1. Material*

The chemicals are $Al(NO_3)_3.9H_2O$ (Merck, 98,5%), NaOH (Merck, 99%), fuming HCl (Merck, 37%), $H_2SO_4$ (Merck, 95-97%), anionic dye is Indigo Carmine manufactured by Merck with molecular weight 466.36 $g.mol^{-1}$, λmax 610 nm, and the structure shown in Fig. 1, fly ash from PT. IPMOMI Paiton Probolinggo, East Java, Indonesia.

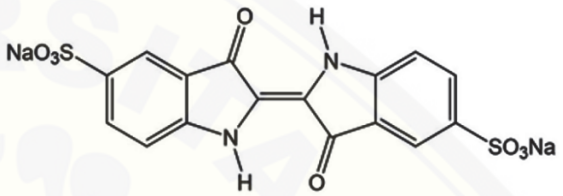


**Fig. 1.** Chemical structure of indigo carmine

### *2.2. Material preparation*

Silica was extracted from 10 g of Fly Ash with NaOH 3 $mol.L^{-1}$ and produced sodium silicate. Sodium silicate titrated with HCl 1 M until pH 7 to form solid silica through the sol-gel process. The soft gel of silica was aged for 18 h, subsequently washed with distilled water and dried at 100 °C for 12 h. Powder of silica gel (SG) produced was calcined at 550 °C for 4 h. SG 5 g was immersed in 50 mL of 10% aluminium solution and stirred for 2 h. Without decantation, the mixture was dried to evaporate the water content and calcined at 550 °C for 4 h to produce modified aluminium onto silica gel (Al/SG).

### *2.3. Material characterization*

The different structure of SG and Al/SG was confirmed by diffractogram of XRD (PANanalytical X'Pert) using Cu-Kα radiation in λ 1,5404 Å with 2θ = 5-50°. FTIR spectra were collected on Shimadzu Prestige 21 at a wavelength of 400–4000 $cm^{-1}$. Surface morphology was studied using SEM FEI Inspect-S50 with 40.000 times magnification and elemental analysis was performed by EDAX AMETEK. Surface area and pore size were determined using Quantachrome Instrument NOVA 1200e.

### *2.4. Indigo carmine adsorption*

A mixture of 25 mL indigo carmine with various concentration (25-500 $mg.L^{-1}$) and 50 mg adsorbent (SG or Al/SG) was placed in a conical flask. The pH of the mixture (2–11) was adjusted by the

addition of 0.1 mol.L$^{-1}$ NaOH or HCl solution. The mixture was shaken for 60 minutes to reach the adsorption equilibrium. The initial and residual concentration of indigo carmine was measured by UV-Visible Spectrophotometer Shimadzu Spectronic 20 at wavelength $\lambda_{max}$ = 611 nm. The adsorption capacity $q_e$ (mg.g$^{-1}$) and efficiency E (%) toward Indigo carmine was calculated as Eqs. (1-2), respectively. The higher adsorption capacity of both adsorbents (SG and Al/SG) was the better as an adsorbent for indigo carmine removal.

$$q_e = (C_0 - C_f)V / m \quad (1)$$

$$E = ((C_0 - C_f)C_0) \times 100\% \quad (2)$$

where: $C_0$ and $C_f$ are respectively the initial and remaining concentration of indigo carmine in mg.L$^{-1}$, $V$ is the volume of the indigo carmine in L and $m$ is the mass of the adsorbent in g.

*2.5. Adsorption isotherm model*

The Isothermal adsorption were evaluated from equilibrium of adsorption data using liniearity models as follows:

*Langmuir Isotherm Adsorption Model*

The model depicts that adsorption occures as a single layer of adsorbed material on homogeneous solid surface. The Linear plot of the Langmuir model can be expressed according to (Eq. 3) by ploting $1/q_e$ vs $1/C_e$.

$$1/q_e = (1/C_e K_L q_{max}) + (1/q_{max}) \quad (3)$$

where: $C_e$ is the equilibrium concentration (mg.L$^{-1}$), $q_e$ is the amount of adsorbed Indigo Carmine on the equilibrium (mg.g$^{-1}$), $q_{max}$ is the complete monolayer sorption capacity (mg.g$^{-1}$), $K_L$ is Langmuir equilibrium constant related to the free energy of adsorption (L.mg$^{-1}$).

Langmuir isotherm of constant separation factor ($R_L$) was used for defining the favorability of the adsorption process. $R_L$ is defined as (Eq. 4); The irreversible isotherm indicated the values of $R_L$ = 0, favorable (0 < $R_L$ < 1), linear ($R_L$ = 1) or unfavorable ($R_L$ > 1).

$$R_L = 1/(1 - bC_0 0) \quad (4)$$

*Freundlich Isotherm Adsorption Model*

The model is appropriate for interaction between adsorbed molecules in multilayer with heterogeneous active sites of the adsorbent. The Freundlich model following linear plot in (Eq. 5) by ploting *Log($q_e$)* vs *Log($C_e$)*.

$$Log(q_e) = \log K_F + 1/nLog(C_e) \quad (5)$$

where: $C_e$ is the equilibrium concentration of adsorbate (mg.L$^{-1}$), $q_e$ is the amount of adsorbate that adsorbed per unit mass (mg.g$^{-1}$), $K_F$ is Freundlich constant related to the adsorption capacity of the adsorbent, $n$ is the Freundlich constants related to surface heterogeneity.

*Temkin Isothermal Adsorption Model*

The models assume that interactions between adsorbate species and adsorbent cause the decreasing linearly of the heat adsorption in the layer of all molecules, and adsorption is characterized by a uniform distribution of binding energies. The model is described as shown in (Eq. 6) by ploting $q_e$ vs ln($C_e$).

$$q_e = \beta \ln Kr + \beta \ln(C_e) \quad (6)$$

where: $\beta = RT/b_t$, where $b_t$ is the Temkin constant related to the heat of adsorption (J.mol$^{-1}$), $K_T$ is equilibrium binding constant (L.g$^{-1}$), $R$ is the universal gas constant (8.314 J.mol$^{-1}$.K$^{-1}$), and $T$ is the temperature of adsorption (K).

*2.6. Adsorption kinetics model*

The studies of kinetics adsorption was calculated by pseudo-first-order, pseudo-second-order, Intra-particle, and Elovich Diffusion Equations models, as follows:

*Pseudo-first-order Model* was determined by the plot between log ($q_e$-$q_t$) versus t, (Eq. 7):

$$Log(q_e - q_t) = Log(q_e) - (k_1 / 2.203) \times t \quad (7)$$

*Pseudo-second-order Model* was determined by plot t/qt versus t, (Eq. 8):

$$t/q_t = 1 + (k_2 \times q_e^{\,2}) + (1/q_e) \times t \quad (8)$$

*Intra-particle Diffusion Model* was determied by plot $q_t$ vs $t^{1/2}$, (Eq. 9):

$$q_t = k_t \times t^{1/2} + C \quad (9)$$

*Elovich Equation Model* was determined by plot $q_t$ vs ln(t). (Eq. 10):

$$q_t = 1/\beta \ln(\alpha\beta) + 1/\beta \ln(t) \quad (10)$$

where: $q_t$ and $q_e$ are the amounts of adsorbate adsorbed in time t and equilibrium (mg.g$^{-1}$), $k_1$ is a constant pseudo-first-order (min$^{-1}$) and $t$ is the interaction time (min), $k_2$ is the Pseudo-second-order costant (g.mg$^{-1}$.min$^{-1}$), $k_t$ is the rate constant of intra-particle diffusion (mg.g$^{-1}$.min$^{-1/2}$) and $C$ showes the relationship boundary layer thickness. The larger of the value of C was the greater of the effect of the barrier layer. α is the adsorption rate constant at first (mg.g$^{-1}$.min$^{-1}$) and parameter β is the relations of the surface that covered and chemisorption activation energy (g.mg$^{-1}$).

## 3. Results and discussion

### *3.1. Characterization of SG and Al/SG*

Metal oxides within fly ash such as $Al_2O_3$, $Fe_2O_3$, CaO, and MgO can reduce adsorption capacity, so purification should be applied. The metal oxides were separated through acid leaching, isolation of $SiO_2$ with NaOH to produce $Na_2SiO_3$ and acidification of $Na_2SiO_3$ result in silica gel. Aluminum impregnation onto silica gel was intended to change the surface charge of silica gel into negative. FTIR spectra show the structural changes caused by modification SG with Aluminium ion. Both SG (Fig. 2.a) and Al/SG (Fig. 2.b) have similar frameworks, i.e., siloxane (Si-O-Si) and silanol (Si-OH). The peaks with a wavenumber of 455, 804, and 1080 $cm^{-1}$ (Peak 3 - 5) indicate the bending, symmetric stretching and asymmetric stretching of the intratetrahedral oxygen atom in Si-O-Si structure.

Meanwhile, the band at 1639 and 3284 $cm^{-1}$ (Peak 1 and 2) are asymmetric stretching and bending of Si-OH. Impregnated $Al^{3+}$ decreased both the peak intensity of 1639 and 1080 $cm^{-1}$ (Peak 2 and 3). The decreased peak in 1639 $cm^{-1}$ of Al/SG was attributed to the interaction between the Si-OH group of the silica surface with impregnated Al, while in 1080 $cm^{-1}$ depicted the $Al^{3+}$ also interacted with Si-O frameworks during the impregnation process. Shin et al. (2004) reported that aluminum ion interacted with Si-OH of silica structure (SBA-15), and also attacked Si-O bonding in the mesoporous framework. Consequently, $Al^{3+}$ were incorporated by reaction with the silanol functional group of silica framework.

Further characterization was carried out by XRD analysis, scanning electron microscope (SEM), and $N_2$ gas adsorption analyzer. Diffraction patterns in Fig. 3 show an inordered structure in both SG and Al/SG. It can lead to the conclusion that the materials are amorphous. The amorphous structure of silica gels can also be found in silica from rice straw (Lu and Hsieh, 2012).

It also indicated the high dispersion of impregnated $Al^{3+}$ in the surface of Silica. The significantly lower intensity of Al/SG than SG on 2θ above 15° (Peak 1) and the peak shifts in 2θ around 25° to 23.5° (Peak 3 to Peak 2) for SG and Al/SG proved the existence of $Al^{3+}$. Hashemian et al. (2014) reported the broad peak at a 2θ angle of around 22° depicted the amorphous structure of silica with a high dispersion of metal ion on its surface. That argumentation was in line with another investigation using the morphology image by SEM in Fig. 4 that shows both SG and Al/SG have irregular sphericle shapes. Since the particle size of Al/SG was bigger than SG, it was indicating that Aluminium was impregnated onto the surface of silica.

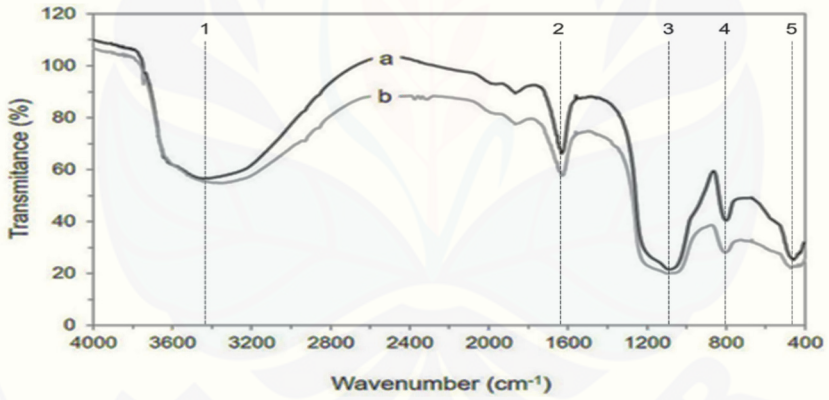


**Fig. 2.** FTIR spectra of SG and Al/SG

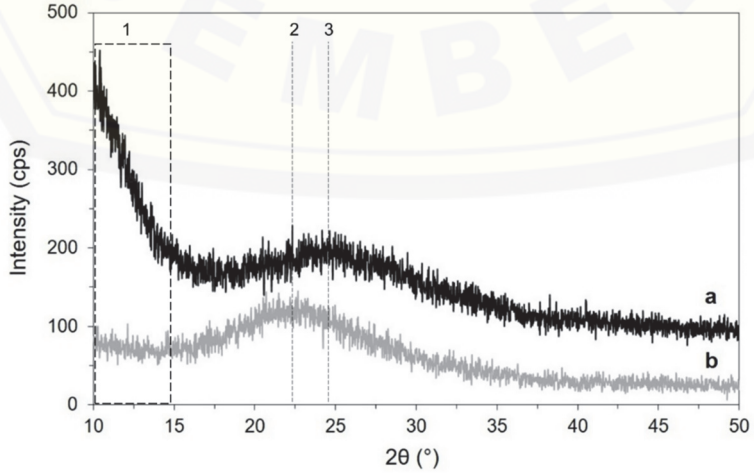


**Fig. 3.** Diffractogram X-ray of SG and Al/SG

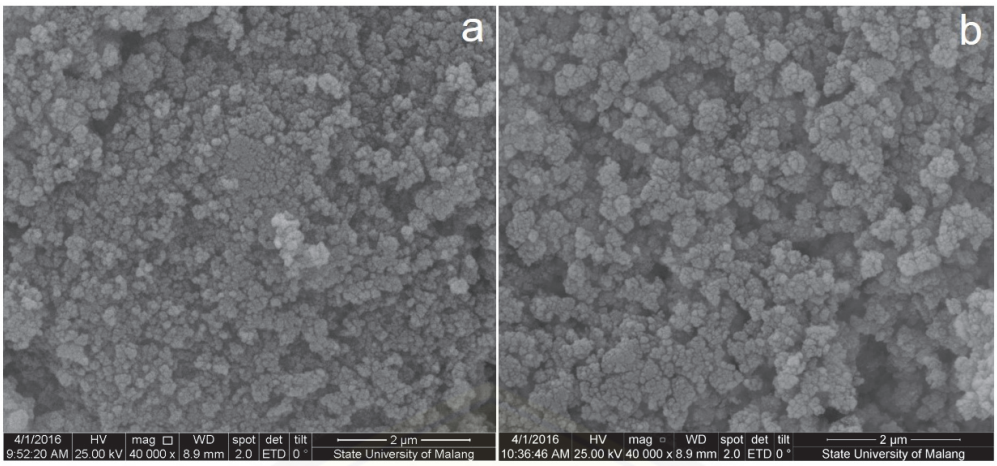


**Fig. 4.** SEM image of a) SG and b) Al/SG

That was also supported by elemental analyses using EDX (Table 1) in increasing of $Al^{3+}$ content in Al/SG compared with SG. Isothermal $N_2$ gas adsorption analyzer profile in Fig. 5. depicted the decreasing of adsorbed $N_2$ gas volume and loop hysteresis in Al/SG than SG. It was affected by the decrease of the surface area and pore volume of Al/SG than in SG (Table 2). Thes most probable phenomena are $Al^{3+}$ block the SG pore and minimize $N_2$ traping in the pore structure of Al/SG.

**Table 1**. Elemental analysis in the adsorbent by EDX

| *Adsorbent* | *Element* | *Wt (%)* |
|---|---|---|
| SG | O | 50.276 |
| | Si | 43.213 |
| | Al | 2.653 |
| | Na | 3.270 |
| Al/SG | O | 49.100 |
| | Si | 44.506 |
| | Al | 6.390 |

**Table 2.** Surface area and pore size analysis of the adsorbent

| *Adsorbent* | *Surface Area ($m^2.g^{-1}$)* | *Pore Size (nm)* | *Pore Volume ($m^2.g^{-1}$)* |
|---|---|---|---|
| SG | 143.55 | 1.909 | 0.279 |
| Al/SG | 125.45 | 1.907 | 0.198 |

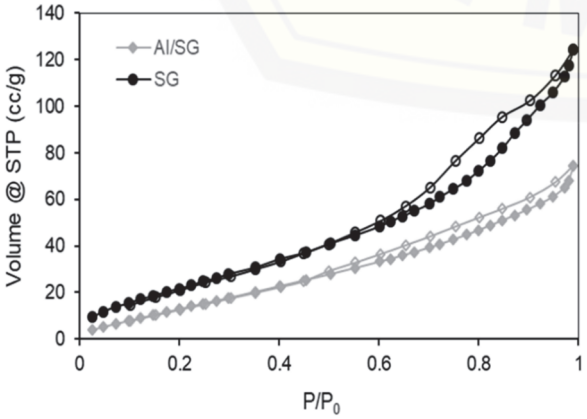


**Fig. 5.** Isothermal ads-Des of $N_2$ curve of the adsorbents

### *3.2. Adsorption studies*

#### *3.2.1. Effect of pH*

One of the important parameters in this adsorption process is the pH of the solution. It affects charge distribution and binding site of both adsorbent and adsorbate (Kamboh et al., 2011). The adsorption was studied in pH of 2-11 with the initial concentration of Indigo carmine of 200 $mg.L^{-1}$ and contact time of 60 minutes. The result is presented in Fig. 6. The highest adsorption capacity of SG and Al/SG toward indigo carmine are achieved at pH 2 and pH 3, respectively. In the acid condition, anionic dye generates a negative charge from the presence of $SO_3^-$ group (Rashwan et al., 2019).

Whereas adsorbent Al/SG has a positive charge that determined from $Al^{3+}$, $[Al(OH)_2]^+$, and $[Al(OH)]^{2+}$, while SG without modification was from $Si\text{-}OH_2^+$. The acid condition may influence anionic exchange between the positive charge on the surface's materials with a negative charge in $SO_3^-$ of a group of dye (Errais et al., 2011). Chen and Chen (2018) also assumed that lower pH enhanced the electrostatic interaction between negative charge of sulfonated groups of indigo carmine and positive charge of adsorbent by the ion exchange. So, the possible interaction between both adsorbent and indigo carmine was represented consecutively in Eqs. (11-12). Moreover, $OH^-$ excess in the solution system caused aluminum in species $[Al(OH)_4]^-$ and the surface of Al/SG has the negative charge, while the negative charge in SG was resulted by protonated silanol group to be $Si\text{-}O^-$. The present of $OH^-$ in the solution system reduced the anion exchange that resulted by electrostatic repulsion force between anionic indigo carmine molecule and negative charge surface of adsorbent (Almoisheer et al., 2019).

Anion Exchange in Al/SG (Eq. 11)

$$Si-O-Al^{3+}X^- + IC^- \rightarrow Si-O-Al^{3+}IC^- + X^- \qquad (11)$$

Anion Exchange in SG (Eq. 12)

$$Si-O-H_2^+X^- + IC^- \rightarrow Si-O-H_2^+IC^- + X^- \qquad (12)$$

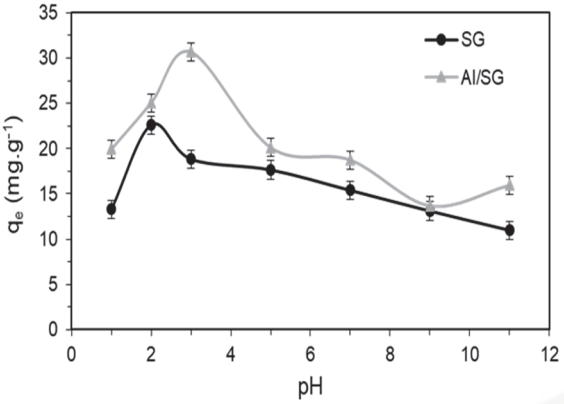


**Fig. 6.** Effect pH system of adsorption indigo carmine

*3.2.2. Effect of initial indigo carmine concentration*

The removal of indigo carmine was examined by different initial concentrations ranging between 25 mg.L$^{-1}$ and 500 mg.L$^{-1}$ in optimum pH systems depicted in Fig. 7.a. The adsorption capacity of SG increased with increasing indigo carmine concentration. The maximum adsorption capacity of SG toward indigo carmine is reached at an initial concentration of 200 mg.L$^{-1}$. These phenomena indicated that the indigo carmine blocked the active site of the adsorbents. Then, the surface of adsorbent is saturated, and as a result, no more adsorbed indigo carmine at higher concentrations. The maximum amount of adsorbed indigo carmine on SG was 25.707 mg.g$^{-1}$ with removal efficiency was 21.82%. Whereas Al/SG has a different profile, the amount of adsorbed indigo carmine increased with increasing initial concentration. However, no plateau profile illustrated the no saturated condition was achieved. In the initial concentration of 200 mg.L$^{-1}$, the amount of adsorbed indigo carmine is 88.143 mg.g$^{-1}$. However, removal efficiency decreased from 98.8 % to 80.47% with the increasing initial concentration of indigo carmine.

*3.2.3. Adsorption isotherms*

The models of adsorption of indigo carmine by SG and Al/SG can be studied using the adsorption isotherm parameters. The adsorption isotherms were fitted by three isothermal equation models, i.e., Langmuir, Freundlich, and Temkin that depicted in Fig. 7. Adsorption isotherms were used for evaluating qualitative information on the adsorption capacity of adsorbents when the adsorption process reaches equilibrium (Tang et al., 2019). Isothermal models are also used to describe the design process of adsorption occurring between indigo carmine and SG or Al/SG. Meanwhile, the adsorption constants of Indigo carmine by SG and Al/SG are calculated and tabulated in Table 3.

**Table 3.** Isothermal model parameters for removal indigo carmine by the adsorbent (adsorbent dosage 50 mg, initial indigo carmine concentration 25-500 mg.L$^{-1}$)

| *Adsorption Models* | *Adsorbents* | |
|---|---|---|
| | *Al/SG* | *SG* |
| $q_e$ exp (mg.g$^{-1}$) | 88.143 | 25.707 |
| **Langmuir** | | |
| $q_{max}$(mg.g$^{-1}$) | 89.286 | 23.679 |
| $K_L$ (L.mg$^{-1}$) | 0.013 | 0.005 |
| $R_L$ | 0.281 | 0.479 |
| $R^2$ | 0.835 | 0.972 |
| **Freundlich** | | |
| $K_F$ (L.g$^{-1}$) | 2.944 | 0.424 |
| $n_F$ | 1.636 | 1.099 |
| $R^2$ | 0.970 | 0.962 |
| **Temkin** | | |
| $b_t$ x 10$^2$ | 0.504 | 3.775 |
| $K_T$ | 3.137 | 22.910 |
| $R^2$ | 0.892 | 0.861 |

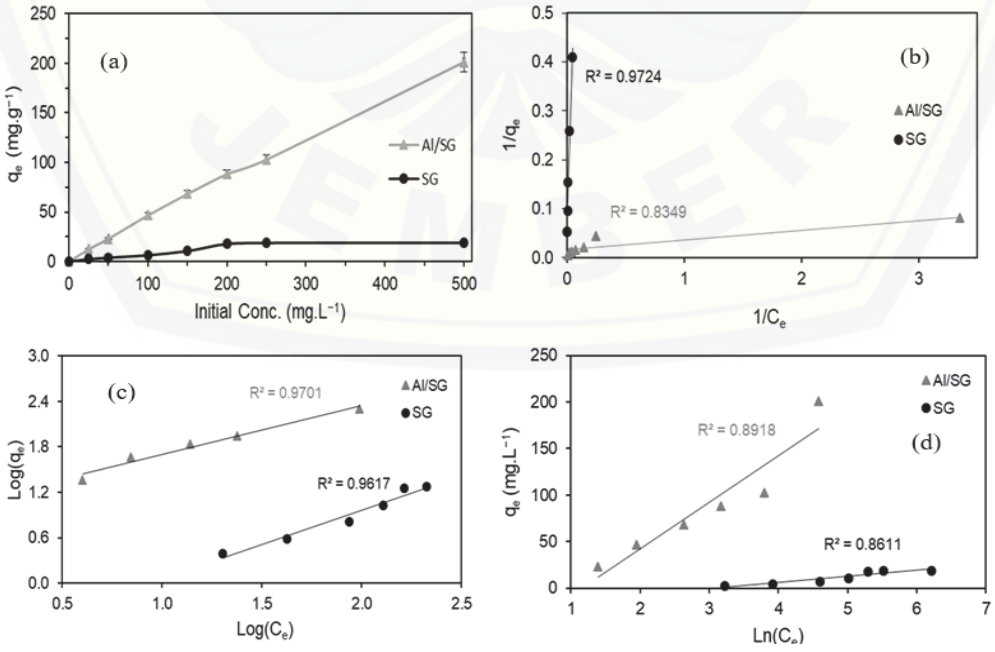


**Fig. 7.** (a) Effect of initial concentration of IC on the adsorption, plot of isotherm adsorption models, (b) Langmuir, (c) Freundlich, (d) Temkin

The adsorption model of SG was best fitted with the Langmuir adsorption isotherm model with the highest coefficient correlation values ($R^2$ = 0.972) as compared with Freundlich ($R^2$ = 0.962) and Temkin ($R^2$ = 0.861). The adsorption process was assumed that indigo carmine adsorbed in the homogeneous surface, and the interactions were the monolayer. The $R_L$ values (0.479) also confirm these phenomena for the SG. This range value ($0 < R_L < 1$) indicates the favorable adsorption isotherm, which followed the Langmuir adsorption isotherm model. The linearity plot of the experimental data was between $1/q_e$ and $1/C_e$ on the variation of the initial concentration that indicated the maximum sorption capacity and Langmuir constant ($q_{max}$ and $K_L$) of the slope and intercepts, respectively. The maximum adsorption capacity, $q_{max}$, of SG was 23.679 mg.g$^{-1}$.

At the same time, the adsorption process of Al/SG could be better matched with Freundlich corresponding with the coefficient correlation ($R^2$ = 0.970) than Langmuir ($R^2$ = 0.835) and Temkin ($R^2$ = 0.892). It indicated the surface site of Al/SG had different binding energy, and the adsorption on the surface of Al/SG was multilayer adsorption from heterogeneous distribution of indigo carmine interaction. The value of the heterogeneity factor (n) was 1.636 (more than 1) that showed the physical and chemical reaction in the adsorption process (Chen and Chen 2018). Multilayer adsorption might be generated from the interaction between the positive charge of adsorbent surface and negative charge from $SO_3^-$ group of indigo carmine, in the acid condition. Moreover, protonated of -NH groups of IC formed -$NH_2^+$ group and facilitated the interaction with another $SO_3^-$ group. The hypotetic interaction between Al/SG and IC depicted in Fig. 8. That showed that impregnation $Al^{3+}$ onto SG significantly increase the adsorption capacity of indigo carmine.

The adsorption capacity of Al/SG and SG, calculated by the three models of adsorption isotherm, were to understand the level of adsorption efficiency. Table 4 listed the adsorption efficiency of the indigo carmine using both adsorbents in comparison with other potential adsorbents from the previous publications. In conclusion, Al/SG had high adsorption efficiency and could be classified as a potential adsorbent to remove indigo carmine.

### *3.2.4. Kinetics of adsorption*

The adsorption kinetics experiments were performed to understand the adsorption diffusion form and the reaction mechanism of indigo carmine on Al/SG and SG. Fig. 9a showed the relationship between contact time and adsorption capacities. According to the figure, the rapid adsorption process was at the beginning, then increased slightly, and finally reached the equilibrium in 60 min for both adsorbent. It was also observed that the adsorption rate of Al/SG was much faster than SG. The adsorption kinetics were analyzed by using pseudo-first-order (Eq. 7), pseudo-second-order (Eq. 8), intraparticle diffusion (Eq. 9) and Elovich (Eq. 10) models. Table 5 shows the relevant parameter of the kinetics models that calculated from each of the slopes and the intercepts of linear regression. The adsorptions indigo carmine on both adsorbent were best expressed using the pseudo-second-order model with the highest correlation coefficients ($R^2$ = 0.99). It indicated that the active site of the adsorbent and molecule of indigo carmine influence in the adsorption process by electron transfer (Sulistiyo et al. 2017; Rashwan et al., 2019).

**Table 4.** The comparison of adsorption capacity of indigo carmine on various adsorbent

| *Adsorbent* | *pH* | *Adsorption Time (min)* | *Initial IC Concentration (mg.L$^{-1}$)* | *Adsorption Capacity (mg.g$^{-1}$)* | *Removal Efficiency (%)* | *Reference* |
|---|---|---|---|---|---|---|
| Calcium Hydroxide | - | 300 | 75 | 0.4 | 58 | Arenas et al. (2017) |
| Zeolite from fly ash | - | 240 | 11 | 1.23 | 90 | Carvalho et al. (2011) |
| Fly ash | - | 45 | 14.7 | 1.48 | 84 | |
| Silica Gel from fly ash | 2 | 60 | 200 | 25.71 | 21.82 | This Study |
| Aluminium/Silica Gel | 3 | | | 88.14 | 80.47 | |
| Fe-zeolitic tuff | 6.5 | 2400 | 200 | 32.83 | - | Gutierrez-Segura et al. (2009) |
| Carbonaceous material from pyrolyzed sewage sludge | | | | 92.83 | - | |
| *Pistia Stratiotes* dry biomass activated $H_2SO_4$ | - | 120 | 200 | 41.2 | 20.6 | Ferreira et al., (2019) |
| Mesoporous Mg/Fe LDH Nanoparticle | 9.5 | 30 | 55.92 | 55.8 | - | Ahmed et al., (2017) |
| Surface modified composite nanofiber | 5 | 120 | 20 | 154.5 | 77.3 | Yazdi et al., (2018) |
| CuAl-LDH | 2 | 360 | 500 | 89.46 | 8.9 | Almoisheer et al. (2019) |
| SWCNTs nanocomposite | | | | 179.5 | 18 | |
| CuAl-LDH/SWCNTs nanocomposite | | | | 294.1 | 29.4 | |

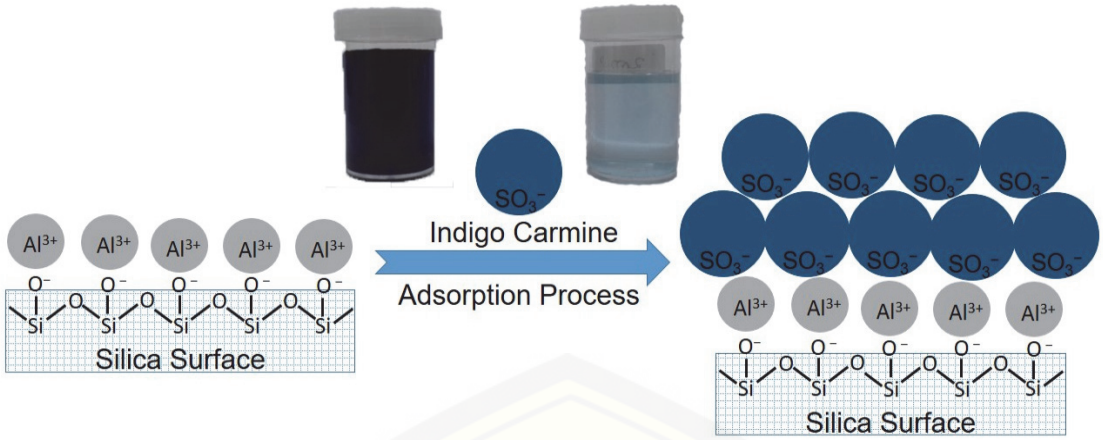


**Fig. 8.** Hypotetical interaction models of IC on Al/SG

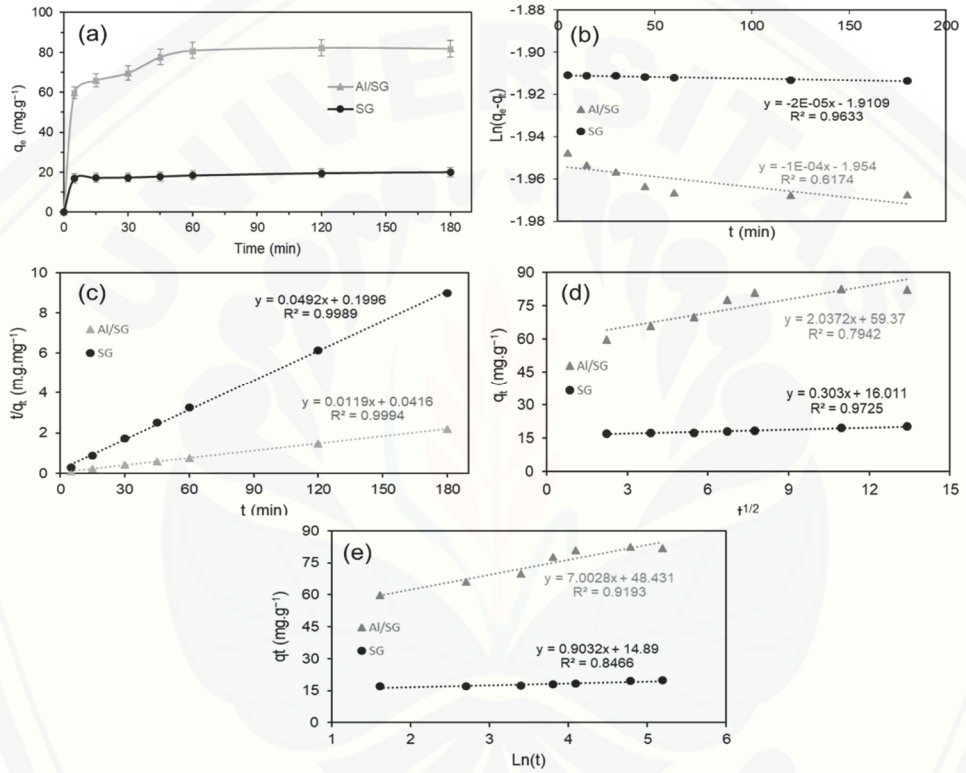


**Fig. 9.** (a) Adsorption kinetics of indigo carmine by adsorbents, plots of (b) Pseudo-first-order, (c) Pseudo-second-order, (d) Intra particle diffusion, (e) Elovich. (200 mg.L$^{-1}$ adsorbate, 50 mg of adsorbents

**Table 5.** Kinetic parameter models of the adsorption of indigo carmine

| ***Kinetic Model*** | ***Parameter*** | ***Al/SG*** | ***SG*** |
|---|---|---|---|
| Pseudo-first-order | $q_e$ (mg.g$^{-1}$) | 1.00 | 1.00 |
| | $k_1$ (min$^{-1}$) | 1.95 | 1.91 |
| | $R^2$ | 0.62 | 0.96 |
| Pseudo-second-order | $q_e$ (mg.g$^{-1}$) | 84.03 | 20.32 |
| | $k_2$.10$^3$ (mg.g$^{-1}$.min$^{-1}$) | 168.94 | 2.10 |
| | $R^2$ | 0.99 | 0.99 |
| Intra-particle diffusion | $k_p$ (mg.g$^{-1}$.min$^{-1/2}$) | 2.04 | 0.30 |
| | $C$ (mg.g$^{-1}$) | 59.27 | 16.01 |
| | $R^2$ | 0.79 | 0.97 |
| Elovich | $\alpha$.10$^4$ (mg.g$^{-1}$.min$^{-1}$) | 0.68 | 1304.63 |
| | $\beta$ (g.mg$^{-1}$) | 0.14 | 1.11 |
| | $R^2$ | 0.92 | 0.85 |

## 4. Conclusions

In conclusion, adsorbent Al/SG was prepared from SG and $Al^{3+}$ using wetness impregnation method for removal indigo carmine as anionic dye representation. Physicochemical properties of adsorbent described that impregnated $Al^{3+}$ covered active site of SG. In consequence, particle size of Al/SG was bigger than SG while the surface area and pore volume decrease.

The adsorption character of Al/SG and SG on indigo carmine was influenced by initial solution pH, initial dye concetration, and contact time. Adsorption isotherms showed that SG and Al/SG consecutively fitted better with Langmuir and Freundlich, which adsorption model following monolayer and multilayer mechanism, respectively.

Adsorption condition was better carried out in pH 2 for SG and pH 3 for Al/SG. The optimum adsorption capacity ($q_{max}$) of both adsorbents was 25.707 mg.g$^{-1}$ and 88.143 mg.g$^{-1}$ in optimal condition 50 mg adsorbent dosage, 200 mg/L$^{-1}$ indigo carmine, 2 h adsorption time. The adsorption kinetic models of SG and Al/SG followed pseudo-second-order model. The result describes that Al/SG can be a potential adsorbent for removal indigo carmine dye from waste water.

## References


Adak D., Sarkar, M., Mandal, S., (2014), Effect of nano-silica on strength and durability of fly ash-based geopolymer mortar, *Construction and Building Materials*, **70**, 453-459.

Ahmed M.A., Brick A.A., Mohamed A.A., (2017), An efficient adsorption of indigo carmine dye from aqueous solution on mesoporous Mg/Fe layered double hydroxide nanoparticles prepared by controlled sol-gel route, *Chemosphere*, **174**, 280-288.

Almoisheer N., Alseroury F.A., Kumar R., Aslam M., Barakat M.A., (2019), Adsorption and anion exchange insight of indigo carmine onto CuAl-LDH/SWCNTs nanocomposite: kinetic, thermodynamic and isotherm analysis, *RSC Advance*, **9**, 560-568.

Alver E., Metin Ü., (2012), Anionic dye removal from aqueous solutions using modified zeolite: Adsorption kinetics and isotherm studies, *Chemical Engineering Journal*, **200-202**, 59-67.

Amir M. Guner S., Yildiz A., Baykala A., (2017), Magneto-optical and catalytic properties of $Fe_3O_4$@HA@Ag magnetic nanocomposite, *Journal of Magnetism and Magnetic Materials*, **421**, 462-471.

Anbia M., Hariri S.A., Ashrafizadeh S.N., (2010), Adsorptive removal of anionic dyes by modified nanoporous silica SBA-3, *Applied Surface Science*, **256**, 3228-3233.

Arenas C.A., Vasco A., Betancur M., Martinez J.D., (2017), Removal of indigo carmine (IC) from aqueous solution by adsorption through abrasive spherical materials made of rice husk ash (RHA), *Process Safety and Environmental Protection*, **106**, 224-238.

Carvalho T.E.M.D, Fungaro D.A., Magdalena C.P., Cunico P., (2011), Adsorption of indigo carmine from aqueous solution using coal fly ash and zeolite from fly ash, *Journal of Radioanalytical and Nuclear Chemistry*, **289**, 617-626.

Chen J., Chen H., (2018), Removal of anionic dyes from an aqueous solution by a magnetic cationic adsorbent modified with DMDAAC, *New Journal of Chemistry*, **42**, 7262-7271.

Costa J.A.S., Paranhos C.M., (2019), Evaluation of rice husk ash in adsorption of Remazol Red dye from aqueous media, *SN Applied Sciences*, **1**, 397-404.

Errais E., Duplay J., Darragi F., M'Rabet I., Aubert A., Huber F., Morvan G., (2011), Efficient anionic dye adsorption on natural untreated clay: kinetic study and thermodynamic parameters, *Desalination*, **275**, 74-81.

Ferreira R.M., De Oliviera N.M., Lima L.L.S., Campista A.L.D.M., Stapelfeldt D.M.A., (2019), Adsorption of indigo carmine on pistia stratiotes dry biomass chemically modified, *Environmental Science and Pollution Research*, **26**, 28614-28621.

Gutierrez-Segura E., Solache-Ríos M., Colín-Cruza A. (2009), Sorption of indigo carmine by a Fe-zeolitic tuff and carbonaceous material from pyrolyzed sewage sludge, *Journal of Hazardous Materials*, **170**, 1227-1235.

Gollakota A.R.K., Volli V., Shu C.M., (2019), Progressive utilisation prospects of coal fly ash: A review, *Science of the Total Environment*, **672**, 951-989.

Hashemian S., Sadeghi B., Mangeli M., (2014), Hydrothermal synthesis of nano cavities of Al-MCF for adsorption of indigo carmine from aqueous solution, *Journal of Industrial and Engineering Chemistry*, **21**, 423-427.

Jiang C., Wang X., Qin D., Da W., Hou B., Hao C., Wu J., (2019), Construction of magnetic lignin-based adsorbent and its adsorption properties for dyes, *Journal of Hazardous Materials*, **369**, 50-61.

Kamboh M.A. Solangi I.B., Sherazi S.T.H., Memon S., (2011), A highly efficient calix[4]arene based resin for the removal of azo dyes, *Desalination*, **268**, 83-89.

Karaca H., Altıntıg E., Turker D., Teker M., (2018), An evaluation of coal fly ash as an adsorbent for the removal of methylene blue from aqueous solutions: kinetic and thermodynamic studies, *Journal of Dispersion Science and Technology*, **39**, 1-8.

Lu P., Hsieh Y.L., (2012), Highly pure amorphous silica nano-disks from rice straw, *Powder Technology*, **225**, 149-155.

Ma J., Cui B., Dai J., Li D., (2011), Mechanism of adsorption of anionic dye from aqueous solutions onto organobentonite, *Journal of Hazardous Materials*, **186**, 1758-1765.

Mahmoodi N.M., Salehi R, Arami M., (2011a), Binary system dye removal from colored textile wastewater using activated carbon: Kinetic and isotherm studies, *Desalination*, **272**, 187-195.

Mahmoodi N.M., Khorramfar S., Najafi F., (2011b), Amine-functionalized silica nanoparticle: Preparation, characterization and anionic dye removal ability, *Desalination*, **279**, 61-68.

Manchanda C.K., Khaiwal R., Mor S., (2017), Application of sol–gel technique for preparation of nanosilica from coal powered thermal power plant fly ash, *Journal of Sol-Gel Science Technology*, **83**, 574-581.

Mishra A., Malik A., (2014), Novel fungal consortium for bioremediation of metals and dyes from mixed waste stream, *Bioresource Technology*, **171**, 217-226.

Rashwan W.E., Abou-El-Sherbini K.S., Wahba M.A., Ahmed S.A.S., Weidler P.G., (2019), High stable Al-MCM-41: structural characterization and evaluation for removal of methylene blue from aqueous solution, *Silicon*, **12**, 2007-2029.

Salleh M.A.M., Mahmoud D.K., Karim W.A.W.A., Idris, A., (2011), Cationic and anionic dye adsorption by agricultural solid wastes: A comprehensive review, *Desalination*, **280**, 1-13.

Shin E.W., Han J.S., Jang M., Min S. H., Park J.W., Rowell, R.M., (2004), Phosphate adsorption on aluminum-impregnated mesoporous silicates: surface structure and behavior of adsorbents, *Environmental Science Technology*, **38**, 912-917.

Silva L.S., Lima L.C.B., Silva F.C., Matos J.M.E., Santos M.R.M.C., Junior L.S.S., Sousa K.S., Filho E.C.S., (2013), Dye anionic sorption in aqueous solution onto a cellulose surface chemically modified with aminoethanethiol, *Chemical Engineering Journal*, **218**, 89-98.

Sulistiyo Y.A., Andriana N., Piluharto B., Zulfikar Z., (2017), Silica gels from coal fly ash as methylene blue adsorbent: isotherm and kinetic studies, *Bulletin of*

*Chemical Reaction Engineering & Catalysis*, **12**, 263-272.

Tang Y., Li M., Mu C., Zhou J., Shi B., (2019), Ultrafast and efficient removal of anionic dyes from wastewater by polyethyleneimine-modified silica nanoparticles, *Chemosphere*, **229**, 570-579.

Wangpradit R., Chitprasert P., (2014), Chitosan-coated Lentinus polychrous Lev.: Integrated biosorption and biodegradation systems for decolorization of anionic reactive dyes, *International Biodeterioration & Biodegradation*, **93**, 168-176.

Yao Z.T., Ji X.S., Sarker P.K., Tang J.H., Ge L.Q., Xia M.S., Xi Y.Q., (2015), A comprehensive review on the applications of coal fly ash, *Earth-Science Reviews*, **141**, 105-121.

Yazdi M.G., Ivanic M., Mohamed A., Uheida A., (2018), Surface modified composite nanofibers for the removal of indigo carmine dye from polluted water, *RSC Advance*, **8**, 24588-24598.

Yuan N., Cai H., Liu T., Huang Q., Zhang X., (2019), Adsorptive removal of methylene blue from aqueous solution using coal fly ash-derived mesoporous silica material, *Adsorption Science & Technology*, **37**, 333-348.

Zhou Y., Lu J., Zhou Y., Liu Y., (2019), Recent advances for dyes removal using novel adsorbents: A review, *Environmental Pollution*, **252**, 352-365.